Long-Wavelength Electromagnetic Power Absorption in Ellipsoidal Models of Man and Animals

HABIB MASSOUDI, MEMBER, IEEE, CARL H. DURNEY, MEMBER, IEEE, AND CURTIS C. JOHNSON, SENIOR MEMBER, IEEE

***Abstract*—A previously developed long-wavelength analysis is applied to ellipsoidal models of humans and experimental animals to obtain the distribution of tissue power absorption and average power absorption for different frequencies and orientations of the model with respect to the field vectors. Curves showing the distribution of absorbed power inside the model, and the average absorbed power versus frequency are presented for several species. Comparisons of calculated data with preliminary experimental data on monkeys are given. The theoretical results show that the power absorption in the ellipsoidal model is a strong function of frequency and orientation with respect to the incident plane wave field vectors. The quantitative data presented here are valuable for estimating tissue electromagnetic (EM) power absorption in experimental animals and humans. These data may also be used in extrapolating EM induced effects measured in animals to those expected in humans.**

I. Introduction

CONCERN for the potential biological hazards resulting from nonionizing electromagnetic (EM) radiation, particularly at microwave and radio frequencies, has increased significantly during the past few years. An important aspect of EM wave biological-effects research involves the investigation of internal electric field strength, internal distribution of EM specific absorbed power, and total specific power absorption in biological tissue subjected to EM irradiation.

The internal distribution of EM fields and specific power absorption in homogeneous spherical models, multilayered spherical models, and anisotropic planar layered models have been investigated, and EM heating in humans has been estimated by measuring the total heat generated in conducting spheres and phantoms of the human body [1]–[10]. The principal results obtained from the theoretical analysis of these models are as follows.

1) Large spatial variations in the internal electric field and specific absorbed power in homogeneous tissue spheres as a function of sphere radius and frequency are predicted. These theoretical results have been confirmed by thermographic camera photographs of irradiated phantom models [1], [7].

2) The resonant frequency is shifted and the peak specific absorbed power is increased in multilayered spherical models compared to homogeneous spherical models.

Manuscript received February 5, 1976; revised June 2, 1976. This work was supported by the U.S. Air Force School of Aerospace Medicine, Brooks Air Force Base, TX 78235.

H. Massoudi is with the Department of Electrical Engineering, University of Utah, Salt Lake City, UT 84112.

C. H. Durney is with the Department of Electrical Engineering and Bioengineering, University of Utah, Salt Lake City, UT 84112.

C. C. Johnson is with the Department of Bioengineering, University of Utah, Salt Lake City, UT 84112.

3) Marked differences in tissue specific absorbed power due to tissue anisotropy at frequencies below 10 MHz are predicted in anisotropic plane layered models.

Although the preceding models have been very valuable in providing considerable insight into the power deposition mechanism and internal field distributions, obtaining more realistic values for local internal power deposition in actual biological systems, such as commonly used laboratory animals, requires more realistic geometrical models. Consequently, a field perturbation approach was applied to prolate spheroidal (cigar shaped with axes $a \neq b = c$) models of humans and experimental animals [11], [12]. This analysis is valid for ka values well below the maximum absorption frequency range. The results show that the internal electric field, the specific absorbed power distribution patterns, and total specific power absorption in the spheroid are strong functions of the orientation of the spheroid with respect to the incident plane wave field vectors, a feature which obviously could not be predicted from the spherical models. This strong dependence of the specific absorbed power upon the orientation of the spheroid with respect to the EM field vectors has been experimentally confirmed [13], [14]. The long-wavelength theoretical results of the prolate spheroid models are in qualitative agreement with recent measurements conducted by Gandhi on different-sized prolate spheroidal phantoms, and different-sized rats in a parallel-plate transmission line [14]. Quantitative comparisons of theoretical results with Gandhi's experimental data have not been possible because his experimental results pertain mostly to higher frequencies centering around the resonant frequency. Allen *et al.*, by means of differential power measurement techniques, have measured the EM power absorption in human and sitting rhesus monkey prolate spheroidal phantoms and in live monkeys, in the frequency range of 10–50 MHz [13], where the perturbation analysis does apply. The theoretical and experimental results for the phantoms are in good agreement. However, Allen and his coworkers found that a 90° rotation of live monkeys about their long axis in the irradiation chamber caused a significant difference in the EM specific power absorption. This effect could not be predicted from the analysis of the prolate spheroidal model because the shape of a prolate spheroid is invariant with rotation about its long axis. These results suggested that an ellipsoidal model (flattened spheroid with $a \neq b \neq c$) would be more appropriate for describing EM specific power absorption in primates. Therefore, the field perturba-

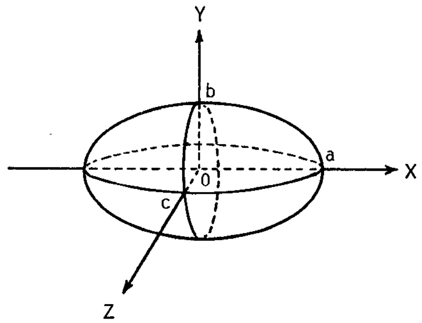

Fig. 1. Orientation of the coordinate system with respect to the ellipsoidal model.

tion technique was applied to a lossy ellipsoidal model, and expressions for internal electric field, internal specific absorbed power distribution, and total specific absorbed power due to an EM plane wave irradiation were derived for the six major orientations of the ellipsoid with respect to the incident plane wave field vectors [15].

In this paper the low ka perturbation theory is applied to ellipsoidal models of different human body types and experimental animals to obtain internal specific absorbed power distribution and total specific absorbed power for different orientations and frequencies. Curves showing the distribution of specific absorbed power inside the body and the average specific absorbed power versus frequency are presented for the ellipsoidal models of several species. The curves confirm that the specific absorbed power is a strong function of the size and orientation of the ellipsoid in the incident fields.

The data presented here are of value in estimating tissue specific power absorption in experimental animals and humans. Furthermore, since the experiments in EM biological effects are performed with animals and since test animals may absorb energy much differently in a given EM field than humans in the same EM field, these data or similar data are essential for extrapolating measured animal biological effects to those expected in humans, and as a guide to establishing an EM radiation safety standard.

II. Theoretical Basis

The equations used in this paper are derived in detail in a previous publication [15]. In that analysis, the ellipsoid is oriented with respect to a coordinate system as shown in Fig. 1, with a plane wave EM field incident upon it in one of the six standard polarizations defined later. Each set of incident, internal, and scattered electric and magnetic fields is expanded in a power series of $(-jk)$, where $j = (-1)^{1/2}$ and k is the free-space propagation constant. Equations for the nth-order field terms are obtained by requiring the series expansions of the incident, scattered, and internal fields to satisfy both Maxwell's equations and the boundary conditions. The dielectric constant and conductivity of the ellipsoidal model were taken from a compilation of data published by Schwan [16] and Johnson and Guy [1]. The variation of the complex dielectric constant with frequency as obtained from these references is given in [12].

Once the tissue electric fields are obtained, the time-averaged specific absorbed power P inside the ellipsoid is calculated from the equation

$$P(x,y,z) = \tfrac{1}{2}\sigma \boldsymbol{E} \cdot \boldsymbol{E}^* \ \mathrm{W/m^3}$$

where σ is the tissue conductivity, $\boldsymbol{E}$ is the vector electric field strength in the tissue, and * denotes the complex conjugate.

In this paper, we use the terminology "specific absorbed power" to mean the "dose rate," "density of rate of absorbed energy," and "density of absorbed power" (often called "absorbed power density"), all of which have units of energy per unit time per unit volume. Furthermore, we will express $P(x,y,z)$ in units of watts per kilogram of tissue mass, assuming a tissue density of 1.0 g/cm^3. The spatial average of $P(x,y,z)$ over the ellipsoid is denoted as P_{av}. The total time-averaged power absorbed by the ellipsoid is $P_{av}V$, where V is the ellipsoid volume, and is given by the volume integral of $P(x,y,z)$ over the ellipsoid.

Solutions are carried out for each of the six primary polarizations, which are defined in terms of which of the vectors $\boldsymbol{E}$, $\boldsymbol{H}$, and $\boldsymbol{K}$ are parallel with the three axes of the ellipsoid. ($\boldsymbol{E}$ is the incident electric field vector, $\boldsymbol{H}$ is the incident magnetic field vector, and $\boldsymbol{K}$ is the incident plane wave propagation vector.) The vector parallel to the longest axis is listed first, the one parallel to the next longest axis is listed second, and the one parallel to the shortest axis is listed last. Thus EHK polarization is the one in which $\boldsymbol{E}$ is parallel to the longest axis (length a), $\boldsymbol{H}$ is parallel to the next longest axis (length b), and $\boldsymbol{K}$ is parallel to the shortest axis (length c). The expressions for $P(x,y,z)$ and P_{av} for the six polarizations are given in [15].

III. Internal Specific Absorbed Power Distribution

In this section the expressions for $P(x,y,z)$ are used to obtain the specific absorbed power distribution along the x, y, and z axes of the ellipsoidal model. We will first consider an ellipsoid with the same height and the same weight as the prolate spheroidal model of humans and briefly compare the internal specific power absorption pattern with that obtained for the prolate spheroidal model by Johnson *et al.* [12].

Fig. 2 shows the relative specific absorbed power along the three axes for EKH polarization. As described in [12], the specific power absorption is caused by an electrically induced $\boldsymbol{E}$ field along the x axis combined with a magnetically induced $\boldsymbol{E}$ field circulating around the z axis. The currents produced by this magnetically induced circulating $\boldsymbol{E}$ field are the familiar eddy currents. The eddy currents circulate in the xy plane, concentrating as they cross the y axis because the path width narrows and weakening as they cross the x axis because the path width broadens. Since the eddy currents are zero on the z axis, the specific absorbed power along the z axis is due solely to the electrically induced $\boldsymbol{E}$ field. The specific absorbed power along the x and y axes is caused by the combination of the electrically and magnetically induced fields. The relatively flat specific absorbed power distribution along the x axis indicates a strong

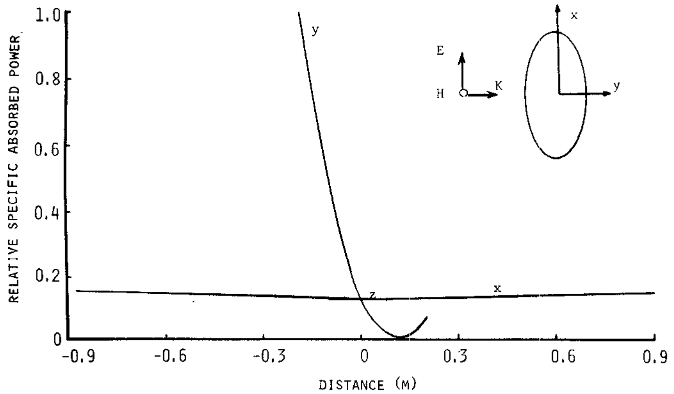

Fig. 2. Relative specific absorbed power along the x, y, and z axes of an ellipsoidal model of man, EKH polarization. $a = 0.875$ m, $b/c = 2$, volume $= 0.07$ m^3, $f = 10$ MHz. The maximum specific absorbed power is 9.08×10^{-3} W/kg for a 1-mW/cm^2 incident plane wave power density.

electrically induced $\boldsymbol{E}$ field, with relatively weak magnetically induced $\boldsymbol{E}$ fields because of the smaller intercepted magnetic flux. The greatly enhanced specific absorbed power along the y axis indicates a predominant electrically induced $\boldsymbol{E}$ field, with peak power absorption on the surface of the ellipsoid first struck by the incident plane wave. The peak specific absorbed power in this case, at 10 MHz, is 9.08×10^{-3} W/kg for a 1-mW/cm^2 incident plane wave power density. This is about 50 percent higher than the peak specific absorbed power in the prolate spheroid model of humans for electric polarization at the same frequency [12], but the pattern of the specific power absorption in the two models is very similar.

Investigation of the equations for $P(x,y,z)$ in the ellipsoidal models of humans and experimental animals shows that for *EKH*, *EHK*, and *HEK* polarizations, the peak specific absorbed power always occurs at the surface of the ellipsoid first intercepted by the plane wave, whereas this is not the case for the *HKE*, *KHE*, and *KEH* polarizations. The location of the peak absorbed power in the last three polarizations depends on the values of a, b, and c, the semiaxes of the ellipsoid. For instance, in the case of *KEH* polarization, the peak specific absorbed power in an ellipsoidal model of humans occurs at $y = \pm b$ (Fig. 1), whereas for an ellipsoidal model of mice, the peak specific absorbed power occurs at $x = +a$, the surface first intercepted by the incident plane wave.

IV. Average Specific Absorbed Power in Animal Models

The average specific absorbed power is calculated for ellipsoidal models of some experimental animals, and the results are given here along with those for humans in Figs. 3–8. These quantitative data will be useful to biological researchers in obtaining estimates of specific power absorbed in the tissue in terms of the incident plane wave power density. Biological effects data may then be correlated with internal specific absorbed power information.

Table I illustrates the average weight, height, and calculated a/b and b/c for the ellipsoidal models of various species compiled from biological references [17]–[19].

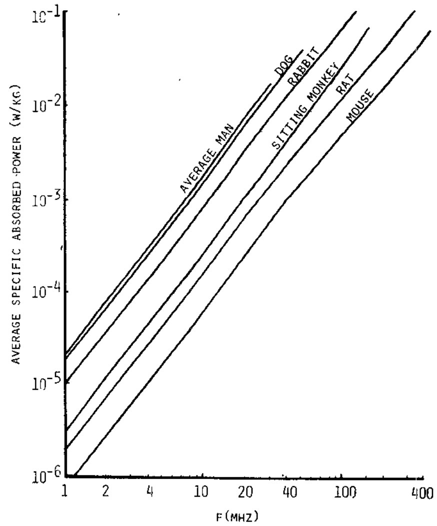

Fig. 3. Average specific absorbed power in ellipsoidal models of man and test animals, *EKH* polarization. Incident plane wave power density is 1 mW/cm^2.

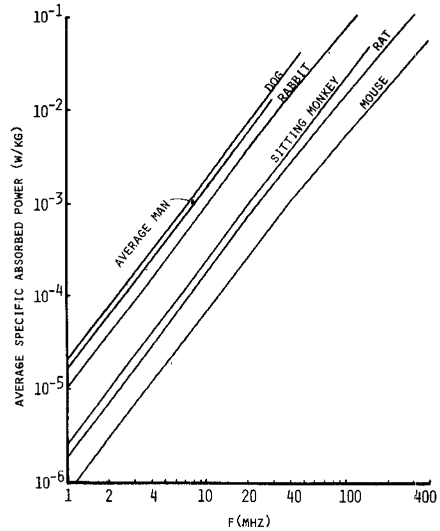

Fig. 4. Average specific absorbed power in ellipsoidal models of man and test animals, *EHK* polarization. Incident plane wave power density is 1 mW/cm^2.

Figs. 3–8 show the average specific absorbed power in ellipsoidal models of humans and test animals for the six standard polarizations for an incident plane wave power density of 1 mW/cm^2. Note that the average specific absorbed power increases approximately as the square of the frequency. The increase would be exactly as the square of the frequency except for the change in dielectric constant with frequency. It should be emphasized that the results given here hold only in the low-frequency range $a/\lambda \lesssim 0.1$. For a human-sized ellipsoid, the theory is valid up to 30 MHz. The frequency range is extended out to 50 MHz for the dog, 150 MHz for the rabbit and the sitting monkey, 400 MHz for the rat, and 1 GHz for the mouse.

It is interesting to note (see Fig. 3) that for *EKH* polarization the average specific absorbed power in man is approximately a factor of 29 times higher than that in a mouse, both for an incident plane wave power density of 1 mW/cm^2.

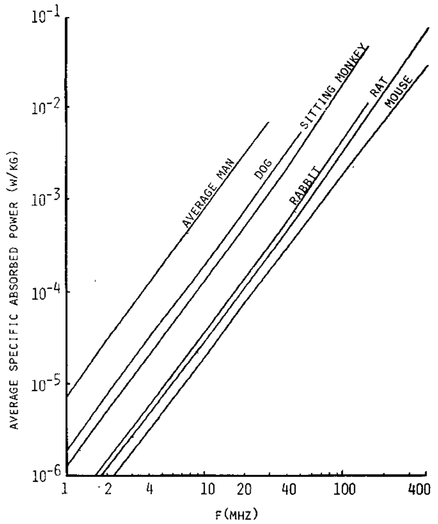

Fig. 5. Average specific absorbed power in ellipsoidal models of man and test animals, *KEH* polarization. Incident plane wave power density is 1 mW/cm².

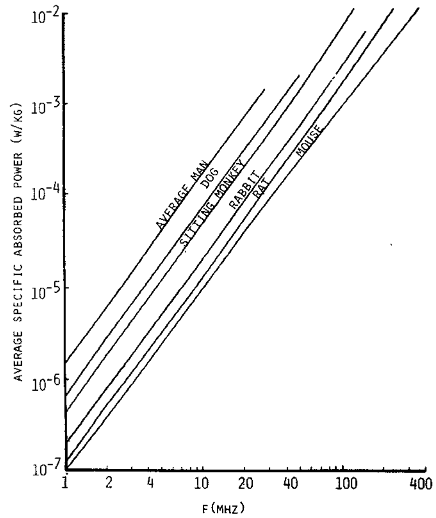

Fig. 8. Average specific absorbed power in ellipsoidal models of man and test animals, *HKE* polarization. Incident plane wave power density is 1 mW/cm².

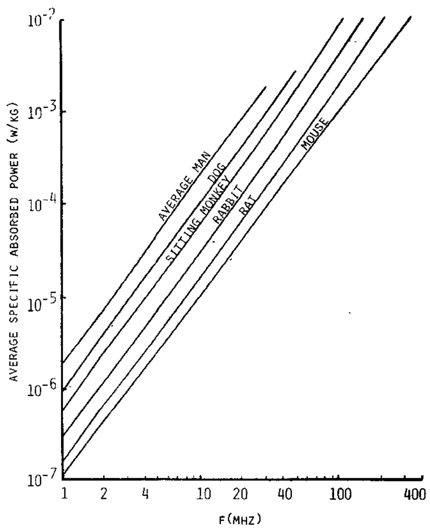

Fig. 6. Average specific absorbed power in ellipsoidal models of man and test animals, *KHE* polarization. Incident plane wave power density is 1 mW/cm².

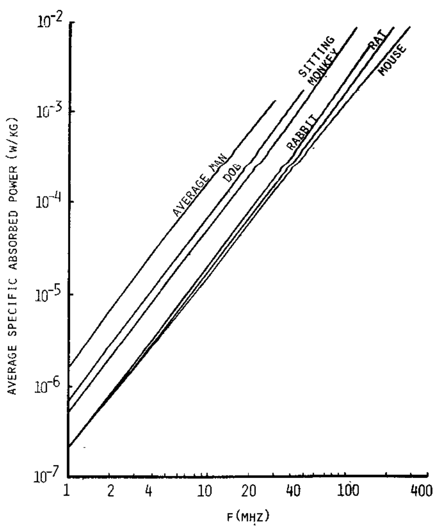

Fig. 7. Average specific absorbed power in ellipsoidal models of man and test animals, *HEK* polarization. Incident plane wave power density is 1 mW/cm².

TABLE I

BIOLOGICAL DATA FOR SEVERAL SPECIES AND THE CALCULATED a/b AND b/c RATIOS FOR THE ELLIPSOIDAL MODEL

Species	Average Weight (kg)	Average Height 2a (m)	a/b	b/c
Average man	70.00	1.75	4.478	2.00
Average woman	61.14	1.61	4.02	2.21
Average ectomorph (skinny) man	47.18	1.76	5.5	2.00
Average mesomorph man	93.26	1.76	4.0	1.91
Average endomorph (fat) man	141.00	1.76	3.92	1.32
10-year old boy	32.2	1.38	4.93	1.84
5-year old boy	19.5	1.12	4.67	1.73
Sitting monkey	3.5	0.4	2.53	1.5
Dog	15.00	1.12	5.92	1.4
Rabbit	1.00	0.4	5.52	1.1
Rat	0.2	0.15	2.54	1.37
Mouse	0.02	0.0536	1.73	1.35

Note: Compiled from [17]–[19].

This means that a mouse will require an incident plane wave power density of about 29 mW/cm² to receive the same average specific absorbed power as a man will at 1 mW/cm². Based upon the preceding comparison, one might conclude that smaller animals absorb less power per unit volume or mass than man, but this is not always true. For example, in Fig. 4, for the *EHK* polarization, the average specific absorbed power in a dog is approximately 13 percent higher than the absorbed power in man. Another interesting example (Fig. 3, *EKH* polarization) is that the average specific absorbed power in a 1-kg rabbit is about three

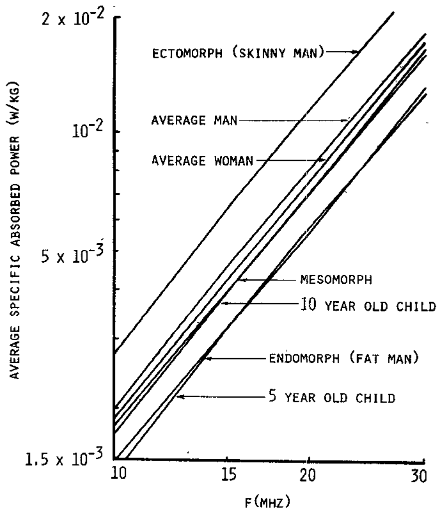

Fig. 9. Average specific absorbed power in ellipsoidal models of different human body types, *EKH* polarization. The incident plane wave power density is 1 mW/cm^2.

times higher than that absorbed by a 3.5-kg sitting monkey, whereas for *KEH* polarization (Fig. 5) the situation is reversed, and the average specific absorbed power in the sitting monkey is higher than that in the rabbit. Notice that the ellipsoidal model of a sitting monkey and that of a rabbit have the same height, but different ratios of a/b and b/c, as shown in Table I. The difference in the specific absorbed power in the preceding examples is first due to the strong orientational effect, which is a critical factor in determining absorbed power, and secondly due to the dependence of the specific absorbed power on the ratios of a/b and b/c, as described in [15]. It can be seen from Figs. 3–8 that for each of the different-sized ellipsoidal models, the average specific absorbed power has the highest value for *EKH* and the lowest value for *HKE* polarization. This is also true for the peak specific absorbed power.

For the polarization with highest power absorption *EKH*, the average specific absorbed power in ellipsoidal models of different human body types is given in Fig. 9. Note that in Fig. 9, among the human models radiated, the value of the absorbed power per unit mass is the highest for the ectomorph (skinny man) and the lowest for the endomorph (fat man). The absorption ratio for these two models is greater than 2:1. This can be explained in terms of electrically and magnetically induced $\boldsymbol{E}$ fields: For *EKH* polarization the electrically induced $\boldsymbol{E}$ field is dominant and the strength of this field is proportional to the ratios of a/b and b/c. The data in Table I indicate that the ellipsoidal models of these men have the same heights ($2a$), but the ectomorph has the highest values of a/b and b/c and therefore absorbs the most energy per unit mass. However, it should be pointed out that this is true only for *EKH* and *EHK* polarizations; for *KEH*, *KHE*, *HEK*, and *HKE* polarizations the situation is reversed. The difference in the specific absorbed power in the ellipsoidal models of children compared to that in the adults is partly due to the difference in the size (lower ka values) and partly due to the differences in the values of a/b and b/c.

The theoretical results for average specific absorbed power in rhesus monkeys are in good agreement with experimental data on live rhesus monkeys [13]. Table II shows a comparison of calculated data with experimental data on monkeys. The model ellipsoid parameters a, b, c, and σ were chosen to give best fit to the data, subject to the condition that the weight of the ellipsoid is equal to the average weight of the monkeys. The relatively good agreement between the theoretical and experimental data indicates that the ellipsoid is a better model than the prolate spheroid, but more work is needed to find the best methods for choosing a, b, c, and σ from measurements of the animal to be modeled.

TABLE II
COMPARISON OF CALCULATED AND MEASURED [13], [20] VALUES OF TOTAL POWER ABSORBED BY 20 LIVE MONKEYS AT 40 MHz

Model Ellipsoid Properties	Polarization	Total Absorbed Power	
		Measured	Calculated
a = .14 m	EKH	847 mW	845 mW
b = .094 m	EHK	832 mW	819 mW
c = .063 m	KEH	376 mW	328 mW
σ = .092 mhos/m	HEK	360 mW	300 mW
	KHE	166 mW	138 mW
	HKE	162 mW	134 mW

V. CONCLUSIONS

A long-wavelength analysis of EM plane wave irradiation of ellipsoidal models of humans and experimental animals has been used to obtain quantitative theoretical estimates of the average specific absorbed EM power and EM power distributions within the model. The EM specific power absorption is found to vary significantly with the orientation of the ellipsoid axis in the incident field vectors, and also with frequency, size, and dielectric properties of the ellipsoid. Theoretical data have been obtained for the average specific absorbed power for six different orientations of the ellipsoid with respect to the incident plane wave field vectors. The strongest absorption is found for the case when the electric field vector of the incident plane wave is along the longest dimension of the ellipsoid.

Within the limits of the ellipsoidal models used to represent humans and animals, these data can be used to extrapolate the results of observed irradiation effects in animals to those expected to be observed in humans. This extrapolation is very important in assessing realistic EM radiation safety levels because the energy absorbed by animals in a given plane wave field can be greatly different from the specific power absorbed by humans in the same plane wave field, and the biological effects due to irradiation are expected to be a function of specific absorbed power.

REFERENCES

[1] C. C. Johnson and A. W. Guy, "Nonionizing electromagnetic wave effects in biological materials and systems," *Proc. IEEE*, vol. 60, pp. 692–718, June 1972.

[2] A. Anne, M. Saito, O. M. Salati, and H. P. Schwan, "Relative microwave absorption cross sections of biological significance,"

in *Biological Effects of Microwave Radiation*, vol. 1. New York: Plenum, 1960, pp. 153–176.
[3] A. R. Shapiro, R. F. Lutomirski, and H. T. Yura, "Induced fields and heating within a cranial structure irradiated by an electromagnetic plane wave," *IEEE Trans. Microwave Theory Tech.* (*Special Issue on Biological Effects of Microwaves*), vol. MTT-19, pp. 187–196, Feb. 1971.
[4] H. N. Kritikos and H. P. Schwan, "Hot spots generated in conducting spheres by electromagnetic waves and biological implications," *IEEE Trans. Biomed. Eng.*, vol. BME-19, pp. 53–58, Jan. 1972.
[5] J. C. Lin, A. W. Guy, and C. C. Johnson, "Power deposition in a spherical model of man exposed to 1–20 MHz electromagnetic fields," *IEEE Trans. Microwave Theory Tech.*, vol. MTT-21, pp. 791–797, Dec. 1973.
[6] W. T. Joines and R. J. Spiegel, "Resonance absorption of microwaves by the human skull," *IEEE Trans. Biomed. Eng.*, vol. BME-21, pp. 46–48, Jan. 1974.
[7] A. W. Guy, "Analysis of electromagnetic field induced in biological tissue by thermographic studies on equivalent phantom models," *IEEE Trans. Microwave Theory Tech.*, vol. MTT-19, pp. 205–214, Feb. 1971.
[8] C. M. Weil, "Absorption characteristics of multilayered sphere models exposed to UHF/microwave radiation," *IEEE Trans. Biomed. Eng.*, vol. BME-22, pp. 468–476, Nov. 1975.
[9] H. N. Kritikos and H. P. Schwan, "The distribution of heating potential inside lossy spheres," *IEEE Trans. Biomed. Eng.*, vol. BME-22, pp. 457–463, Nov. 1975.
[10] C. C. Johnson, C. H. Durney, and H. Massoudi, "Electromagnetic power absorption in anisotropic tissue media," *IEEE Trans. Microwave Theory Tech.*, vol. MTT-23, pp. 529–532, June 1975.
[11] C. H. Durney, C. C. Johnson, and H. Massoudi, "Long-wavelength analysis of planewave irradiation of a prolate spheroid model of man," *IEEE Trans. Microwave Theory Tech.*, vol. MTT-23, pp. 246–253, Feb. 1975.
[12] C. C. Johnson, C. H. Durney, and H. Massoudi, "Long-wavelength electromagnetic power absorption in prolate spheroidal models of man and animals," *IEEE Trans. Microwave Theory Tech.*, vol. MTT-23, pp. 739–747, Sept. 1975.
[13] S. J. Allen, W. D. Hurt, J. H. Krupp, J. A. Ratliff, C. H. Durney, and C. C. Johnson, "Measurement of radio-frequency power absorption in monkeys, monkey phantoms, and human phantoms exposed to 10–50 MHz fields," in *Proc. 1975 Annu. USNC/URSI Meeting* (Boulder, CO), Oct. 1975, p. 200.
[14] O. P. Gandhi, "Frequency and orientation effects on whole animal absorption of electromagnetic waves," *IEEE Trans. Biomed. Eng.*, vol. BME-22, pp. 536–542, Nov. 1975.
[15] H. Massoudi, C. H. Durney, and C. C. Johnson, "Long-wavelength analysis of plane wave irradiation of an ellipsoidal model of man," this issue, pp. 41–46.
[16] H. P. Schwann, "Electrical properties of tissues and cells," *Advan. Biol. Med. Phys.*, vol. 5, pp. 147–209, 1957.
[17] *Collier's Encyclopedia*, vol. 19.
[18] *Encyclopedia Britannica*, vol. 7.
[19] H. Dreyfuss, *The Measure of Man, Human Factors in Design*, Whitney Library of Design, New York, 1967.
[20] S. J. Allen, W. D. Hurt, J. H. Krupp, J. A. Ratliff, C. H. Durney, and C. C. Johnson, "Measurement of radio frequency power absorption in monkeys, monkey phantoms, and human phantoms exposed to 10–50 MHz fields," Report SAM-TR-76-5, USAF School of Aerospace Medicine, Aerospace Medical Division (AFSC), Brooks Air Force Base, TX 78235.

Short Papers

New Method for Computing the Resonant Frequencies of Dielectric Resonators

TATSUO ITOH, SENIOR MEMBER, IEEE, AND RONALD S. RUDOKAS, STUDENT MEMBER, IEEE

***Abstract*—A new method is developed for accurately predicting resonant frequencies of dielectric resonators used in microwave circuits. By introducing an appropriate approximation in the field distribution outside the resonator, an analytical formulation becomes possible. Two coupled eigenvalue equations thus derived are subsequently solved by a numerical method. The accuracy of the results computed by the present method is demonstrated by comparison with previously published data.**

I. Introduction

Dielectric resonators made of high permittivity material have found practical applications in microwave circuits due mainly to their high-Q values. The dominant $TE^{\circ}_{01\delta}$ mode in the low-profile cylindrical resonators [Fig. 1(a)] has traditionally been analyzed by using the so-called magnetic wall model, in which the cylindrical surface containing the circumference of the resonator is replaced with a fictitious open-circuit boundary (magnetic wall) [1]. Recently, Konishi *et al.* [2] reported a more accurate method based on the variational procedure for computing the resonant frequency of $TE^{\circ}_{01\delta}$ modes. Their predicted resonant frequencies agree with experimental data within 1 percent [2]. On the other hand, the magnetic wall method typically gives rise to numerical values smaller than the experimental by about 10 percent.

The method reported by Garault and Guillon [4] is also capable of predicting the resonant frequency with less than 1 percent error. In their method, successive application of imperfect magnetic wall conditions on side and end walls results

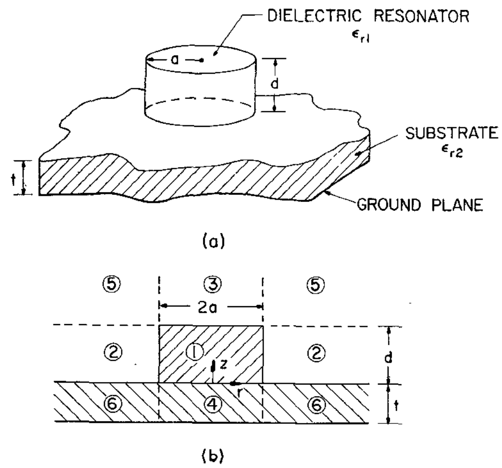

Fig. 1. (a) Dielectric resonator. (b) Side view of dielectric resonator.

Manuscript received April 1, 1976; revised June 28, 1976. This work was supported in part by U.S. Army Research Grant DAHC04-74-G0113 and in part by Joint Services Electronics Program DAAB07-72-C-0259.

T. Itoh was with the Department of Electrical Engineering and the Coordinated Science Laboratory, University of Illinois, Champaign/Urbana, IL 61801. He is now with the Stanford Research Institute, Menlo Park, CA 94025.
R. S. Rudokas was with the Department of Electrical Engineering and the Coordinated Science Laboratory, University of Illinois, Champaign/Urbana, IL 61801. He is now with the Electromagnetic Systems Laboratory Inc., Sunnyvale, CA 94086.